EFDA–JET–CP(11)04/34

S. Wiesen, S. Brezinsek, A. Järvinen, T. Eich, W. Fundamenski, A. Huber,
V. Parail, G. Corrigan, N. Hayashi and JET EFDA contributors

Integrated Modelling of a JET Type-I ELMy H-mode Pulse and Predictions for ITER-Like Wall Scenarios

Integrated Modelling of a JET Type-I ELMy H-mode Pulse and Predictions for ITER-Like Wall Scenarios

S. Wiesen[1], S. Brezinsek[1], A. Järvinen[2], T. Eich[3], W. Fundamenski[4], A. Huber[1], V. Parail[4], G. Corrigan[4], N. Hayashi[5] and JET EFDA contributors*

JET-EFDA, Culham Science Centre, OX14 3DB, Abingdon, UK

[1]Institut für Energie- und Klimaforschung – Plasmaphysik, EURATOM Association Forschungszentrum Jülich, D-52425 Jülich, Germany
[2]Aalto University, Association EURATOM-Tekes, P.O.Box 4100, 02015 Espoo, Finland
[3]Max-Planck-Institut fur Plasmaphysik, EURATOM-Association, D-85748 Garching, Germany
[4]EURATOM-CCFE Fusion Association, Culham Science Centre, OX14 3DB, Abingdon, OXON, UK
[5]Japan Atomic Energy Agency, Naka, Ibaraki-ken 311-0193, Japan
** See annex of F. Romanelli et al, "Overview of JET Results", (23rd IAEA Fusion Energy Conference, Daejon, Republic of Korea (2010)).*

Preprint of Paper to be submitted for publication in Proceedings of the
38th EPS Conference on Plasma Physics
Strasbourg, France
(27th June 2011 - 1st July 2011)

ABSTRACT

A baseline type-I ELMy H-mode discharge in JET (Pulse No: 73569) in low triangularity has been analysed numerically using the JINTRAC integrated code suite in order to obtain a self-consistent description of the edge and core plasma. The time-dependent model consists of a self-consistent coupling of the core plasma dynamics utilising the 1D core code JETTO/SANCO and the 2D multi-fluid Scrape-Off-Layer (SOL) code EDGE2D-EIRENE. The inter- and intra-ELM transport model of JINTRAC has been adapted to match the experimental pre- and post ELM plasma profiles measured by high-resolution Thomson scattering in JET and at the same time the observed ELM dynamics in terms of ELM frequency, ELM energy loss, ELM wetted area and heat flows towards the target plates. It is found that the scaling for the free streaming approximations of ELM filamentary parallel SOL transport for the maximum heat flux, energy density and heat flux factor can be reproduced with the JINTRAC model. The results for the JET all-carbon device reference case are then utilised to predict a type-I ELMy H-mode for the JET ITER-Like Wall (ILW) assuming a full-tungsten divertor and beryllium main-chamber wall in the model. By keeping all transport relevant parameters fixed for the inter- and intra-ELM phase it is found that a moderate amount of seeded neon impurity (or other impurity species) is necessary to match a similar level of radiation when carbon is absent in the system. Finally, the results of the ILW setup are used to estimate the total amount of tungsten particles eroded per ELM from the target plates and a rough estimate of the core radiative fraction due to W accumulation is given.

1. INTRODUCTION

ITER as the next step fusion device requires to deploy tungsten as divertor plasma-facing material to qualify for D-T plasma operational safety limits with respect to tritium retention. For the envisaged ITER baseline H-mode scenario the target Plasma-Facing Component (PFC) has to bear heat loads of the order 10-20 MW/m^2 between ELMs and several hundreds of MW/m^2 for the short period of the actual ELM phase. Tungsten can be eroded by other wall-material impurities like beryllium and much stronger by seeded impurities due to their higher mass. Thus an understanding of the impurity composition and transport in particular during the dominant physical sputtering intra-ELM phase is essential due to its ultimate effect on the core plasma performance.

At JET the ITER-Like Wall (ILW) experiments [1] will be executed starting in 2011. During the 2010/11 shutdown the C first wall material is replaced by Be in the main chamber and W in the divertor. Detailed preparatory work has been conducted in order to be on the one hand prepared for the plasma operation within new limitations and on the other hand to provide reference plasmas for comparison and predictive modelling [2]. With the ILW, carbon as the main intrinsic impurity radiator in the divertor is missing and needs to be replaced by seeded impurities to ensure sufficient power exhaust by radiation cooling and to reduce the tungsten source by physical sputtering to ensure long lifetime of components. Whilst with all-C PFCs chemical- and physical sputtering determines the wall erosion process, it is solely physical sputtering of Be and W by D, seeded and

intrinsic impurities prevalent in the new wall combination.

To assess the fairly new operational regimes for the ILW, firstly, the numerical analysis of a typical JET type-I H-mode scenario (JET Pulse No: 73569, gas fuelled, $\delta = 0.2$, $I_p = 2.2$MA, $B_t = 2.2$T, $P_{NBI} = 13$MW, $n = 0.75 n_{GW}$, no impurity seeding) with an all-carbon wall using the integrated code suite JINTRAC is presented in section 2. To validate the numerical parameters used for the plasma transport and ELM characteristics the time-wise evolution of pedestal plasma and target heat-flux profiles are compared with experimental data from high-resolution Thomson scattering diagnostics, bolometry and IR target camera. Furthermore the model parameters for the adhoc ELM-characteristics are varied and the results are compared with the free-streaming approach for ELM-filamentary transport in the SOL.

In section 3, the results for the all-C reference case are taken, transferred to the ILW and predictively analysed with JINTRAC. Be erosion and transport from the main-chamber wall into the divertor as well as the ramification on the W sputtering by Be and seeded impurities (remaining C can within this approach also be described as 'seeding' impurity species) are discussed. With W sputtered mainly at the ELM-phase the W-erosion influx is calculated and an estimate of the tungsten core concentration and radiative fraction is finally presented.

2. TIME-DEPENDENT JINTRAC MODEL FOR A LOW-TRIANGULAR ALL-CARBON JET ELMY H-MODE REFERENCE DISCHARGE

JINTRAC [3] (formerly known as COCONUT [4]) combines the 1.5D core fluid code JETTO/SANCO [5,6] and the 2D multi-fluid edge code EDGE2D-EIRENE [7-9] by exchanging heat and particle fluxes crossing the separatrix between the two codes. Additionally, plasma transport coefficients derived from JETTO at the plasma edge are communicated to EDGE2D-EIRENE and subsequently, EDGE2D-EIRENE returns the neutral fluxes from the SOL and divertor into the confined region. By using this approach a self-consistent time-dependent solution for both core and SOL plasma can be achieved.

2.1. JINTRAC TRANSPORT MODEL

The equilibrium used in the modelling for JET discharge JET Pulse No: 73569 ($I_p = 2.2$MA, $B_t = 2.2$T, $\delta = 0.2$, cf. fig.1) was fixed in time and processed through a magnetic equilibrium reconstruction (EFIT) into JINTRAC. The JETTO core fluid equations for plasma density, temperature and current (including bootstrap fraction) are solved on a 1D discretised radial grid up to the separatrix where in the presented analysis the feedback of the current on the equilibrium was precluded. For the JET Pulse No: 73569 reference scenario a constant auxiliary power of P_{NBI}=13MW was applied by using the neutral beam model PENCIL [10] of JETTO.

For the anomalous transport in JETTO the empirical Bohm/gyroBohm scaling model adapted to JET conditions [11] was used. The neoclassical part was treated by using the NCLASS package [12]. An edge transport barrier (ETB) was imposed having a fixed reference extent of 3-4 cm

mapped at the outer midplane. The anomalous transport in the ETB is suppressed and fixed by a finite level of radial transport of the order of neo-cassical level for the ion heat conductivity $\chi_i^{ETB} = 0.15\ m^2/s$. Electron heat conductivity and mass diffusion are governed by residual levels of turbulence and values for χ_e^{ETB} and D^{ETB} are defined in an adhoc way to match the pedestal heights seen in the experiment. In order to recover roughly the observed pre-ELM top pedestal heights $T_e^{ped} = 1000eV$, $n_e^{ped} = 4\text{-}5\ 10^{19}\ m^{-3}$ (cf. fig1) and ELM frequency $f^{ELM} \sim 15Hz$ the following values have been selected: $\chi_e^{ETB} = 0.08\ m^2/s$, $D^{ETB} = 0.15\ m^2/s$.

The MHD destabilising effect of ELMs can be included in JINTRAC by a variation of different models [13,14]. Here, a rather adhoc purely ballooning model for the ELM characteristics was assumed. From the HRTS system at JET a maximum allowable normalised ETB pressure gradient $\alpha = 2\mu_0 q^2/B^2(dp/d\rho)$ was derived. The critical limit $\alpha_{crit} = 1.6$ was thus prescribed into JETTO at which an ELM shall be triggered. The ELM itself is characterised by a strong enhancement of the radial transport by imposing a Gaussian shape of radial transport coefficients for a short time $\tau^{ELM} = 200\mu s$ centrally located at $r/a = 0.97$ and a given radial width Δ^{ELM} and maximum values $D^{ELM}, \chi_i^{ELM}, \chi_e^{ELM}$. Such a short and strong increase of transport will release the plasma content from the edge almost instantaneously into the SOL. The values for these ELM parameters were not derived by first principles (i.e. no MHD stability analysis was pursued within JINTRAC) but rather selected to match the ELM dynamics as seen in the experiment.

The coupled 2D SOL radial transport model EDGE2D-EIRENE receives particle and heat fluxes from JETTO. In earlier attempts to model JET ELMy H-mode discharges with multi-fluid plasma edge codes [15,16] it was suggested that a prolongation of the zone with suppressed anomalous transport into the near-SOL helps to match the measured SOL profiles and radial heat flux widths λ_q. Thus, also here the level of transport at the separatrix provided by JETTO was taken and used to reduce transport a few millimeters outward (2-3mm at the outer midplane and mapped poloidally along flux surfaces) into the SOL. Further out into the far SOL the transport was increased to some Bohm-like level of anomalous transport: $D^{far-SOL} = \chi_{i,e}^{far\text{-}SOL} = 0.2 m^2/s$. In case of an ELM-crash the enhanced transport due to the ELM is radially prolonged into the SOL and the level of transport is assumed to decay exponentially to lower levels in the far-SOL and thus not to overestimate heat and particle loads to the main chamber walls. The parallel transport in EDGE2D is assumed to be classical. Kinetic corrections using heat- and viscosity flux limiters could have been applied too, but the overeall effect of these was only limited and affected the ratio between electron and ion heat actually arriving at the targets. The total amount of heat was exclusively dependent on the upstream energy exhaust. The particle, momentum and energy sources and sinks due to neutral recycling and plasma-wall interaction in EDGE2D are derived by the kinetic Monte-Carlo code EIRENE. Physical sputtering [17] and the chemical erosion of carbon [18] have been included. A cold neutral molecular deuterium gas-puff was applied above the inner baffle of the JET vessel in the model (cf. fig.1) with a constant rate of $0.9 \cdot 10^{22}$ el/s (in the experiment the gas fuelling was applied at the inner

vertical target). Additionally, a seeded neon atomic gas flux was applied (cf. section 3). All neutral fluxes eventually crossing the separatrix into the confined region are taken over by the JETTO code which approximates the particle sources from neutrals by a fluid-treatment [19].

Both codes JETTO/SANCO and EDGE2D-EIRENE were dealing with deuterium bulk species, neon seeding and carbon intrinsic impurity (or beryllium to replace carbon in case of the ILW, cf. section 3).

2.2. PEDESTAL DYNAMICS AND ELM HEAT LOAD SCALINGS

The nature of the ELM crash has to be evaluated by utilising a non-linear MHD stability analysis. Pamela et al [20] presented the results of a proper nonlinear MHD stability analysis of the JET Pulse No: 73569 with the JOREK code. But the definition of the ELM in JINTRAC is done adhoc by specifying Gaussian profile widths Δ^{ELM} and amplitudes of heat conductivities and diffusivities (D^{ELM}, χ_i^{ELM}, χ_e^{ELM}) and these cannot be directly deduced from the JOREK code. Rather one has to scan through variations of these quantities and compare them to the experimental data for pedestal drops $\Delta T/T$ and $\Delta n/n$ as well as heat loads towards the target plates and ELM wetted area A_{wet}.

The best match when comparing to pre- and post-ELM experimental profiles taken from HRTS diagnostics (fig.1, cf. [21]) and ELM frequency was ultimately achieved by making the ELM more convective, i.e. by increasing radial D^{ELM} to high values:

W^{ELM} [kJ]	χ_i^{ELM} [m^2/s]	χ_e^{ELM} [m^2/s]	D^{ELM} [m^2/s]	Δ^{ELM} [mm]	Δn_e [$10^{19} m^{-3}$]	T_e [eV]	f^{ELM} [Hz]	q_{max} [MW/m^2]
275	300	100	200	80	0.7	500	26	540
371	300	100	750	80	1.0	500	19	294
466	300	100	1250	80	1.3	500	16	213

Figure 2 displays the JINTRAC modelled pedestals for n_e and T_e before and after the ELM crash as well as their corresponding pedestal drops for the three ELM characteristics in the table above to be directly compared with the experimental profiles in fig. 1. With increasing D^{ELM} the density pedestal drop Δn increases, W^{ELM} increases and the ELM frequency f^{ELM} decreases as expected ($f^{ELM,exp}$~15 Hz). The experimental peak value of $\Delta n=1.5\ 10^{19}\ m^{-3}$ is roughly achieved in case of the ELM with largest size $W^{ELM} = 466$kJ. However, this value for W^{ELM} when compared to the experimental measurement $W^{ELM,exp}$~240kJ is in fact an overestimate. Although the pre- and post-ELM profiles for n_e and T_e can be roughly recovered (apart from the concavity of the post-ELM density profiles as seen in fig. 2 which is accounted to the purely diffusive nature of ELMs in JINTRAC) further optimisation of the ELM characteristic is necessary, yet difficult, since a measurement of ion temperature profiles with high time-resolution was not available and thus the exact value for ion heat conductivity χ_i^{ELM} remains an uncertainty.

The infra-red diagnostics system for the JET outer horizontal target has a good time- and spatial resolution. Fig. 3 compares the IR measurement timewise evolution of the integrated power P(t) arriving at outer target with the JINTRAC results of the three cases described above. The experimental peak power of 50MW is overestimated in JINTRAC by several factors (e.g. factor 8 for the $W^{ELM} = 275$kJ case). However, the power decays much faster in JINTRAC within 0.5ms compared to 4ms in the experiment and thus the total energy arriving at the target integrated over time is rather similar (see also discussion on target energy density scaling below). Moreover, the code maintains the power balance and shows a power asymmetry between inner- and outer target of 2/3 and 1/3 respectively which is generally observed in experiment either [22]. In Fig.3 the JINTRAC heat load profiles for the outer horizontal target are plotted showing as an example results of the largest ELM case $W^{ELM} = 466$kJ. The inter-ELM heat load with a peak of $10MW/m^2$ is well reproduced. But as for the power at the ELM-crash the heat load is again overestimated by several factors (in this case factor 4) whereas an approximate FWHM of ~5cm for the first peak of the heat flux profiles is roughly matching the experimental value.

For the three JINTRAC cases discussed above Fig.3 displays the transients of the ELM wetted area $A_{wet}(t) = P(t)/q_{max}(t)$ at the outer horizontal target where $q_{max}(t)$ is the maximum value of total heat flux and compares them with the experimental transient measured by IRTV. In JINTRAC A_{wet} peaks at the time when the ELM energy arrives at the target and decays quickly within 0.5ms. The peak value A_{wet}~0,90 m^2 compares fairly with the experiment $A_{wet,exp}$~1.2 m^2 (the latter being the gross value including heat from the background, the actual value is ~20% lower as described in [23]). In JINTRAC a second peak appears at 7-8ms after the ELM crash which can be attributed to the background. Generally, this feature of a double peaking of A_{wet} has been found experimentally as reported also in [24]. But the time lag between the first peak and the broader secondary peak is much longer in JINTRAC which is attributed to the much faster power decay in the SOL.

From these results so far we conclude that the actual definition of the ELM characteristics has a stronger impact on the edge particle and heat exhaust and transport into the divertor than on the pedestal height. The latter is largely correlated with the inter-ELM transport assumption D^{ETB} and $\chi_{i,e}{}^{ETB}$ and the MHD stability limit in terms of critical pressure gradient α_{crit}. The bar chart in Fig.4 displays the variation of all the ELM-characteristics used in the JINTRAC modelling presented (α_{crit}=1.6 constant). Generally, the ELM energy loss can be changed not only by modifying its ELM induced diffusivity D^{ELM} but also its conductivity χ^{ELM} and ELM penetration depth Δ^{ELM}. A_{wet} does actually change with ELM energy as shown in Fig. 4 and a linear dependence of A_{wet} for the lower range of W^{ELM} can be recovered. But this linearity seems to be observable only for the cases where D^{ELM} is of the order of the conductive channel, i.e. $D^{ELM} \sim \chi_{i,e}{}^{ELM}$. Increasing D^{ELM} while keeping conductivity $\chi_{i,e}{}^{ELM}$ strongly increases W^{ELM} but saturates A_{wet}. The strongest impact on A_{wet} is observed due to a change in ELM penetration depth Δ^{ELM}.

The free streaming approximation of ELM filamentary transport in the SOL [25] suggests that quantities like the maximum of the heatflux q_{max} and energy density ε depend solely on parallel

transport times and lengths as well as on pedestal pressure, temperature and ion mass (i.e. on sound speed c_s^{ped}). From kinetic PIC simulations for typical JET ELMy H-mode scenarios with large 400kJ ELMs [26,27] normalised quantities $q_{max}^{norm} = \max(q(t))/p^{ped} c_s^{ped} \min(1,\tau_{ELM}/\tau_{||}) \sim 0.56$ and $\varepsilon^{norm} = \int_{t_{ELM}}^{t_{ELM}+\tau_{ELM}} P(t)dt \Big/ L_{||} p^{ped} \sim 0.6$, were derived where τ_{ELM} is the duration of the ELM (i.e. the period until heatflux at target decays below 10% of its maximum) and $\tau_{||} = L_{||}/c_s^{ped}$. Values of the same range were derived using a 1D fluid model for the SOL [28]. JINTRAC values as seen from Fig. 4 are of the same order and specifically the experimental value for the energy density $\varepsilon^{norm,exp}$ ~0.35 as measured by outer target IR diagnostics for JET Pulse No: 73569 is recovered quite well whereas q_{max}^{norm} is generally too high for simulated cases compared to experiment ($q^{max,exp}$~0.2) and a strong dependence is observed with ELM penetration depth Δ^{ELM} and strong ELM diffusivity D^{ELM}. The simplest explanation for this is the much shorter ELM target power decay time in JINTRAC $\tau_{ELM,JINTRAC}$~0.5ms compared to the experimental value $\tau_{ELM,exp}$~4ms. The SOL fluid model in JINTRAC obviously transports the ELM induced upstream energy and particle source too fast downstream. But integrated over time the energy balance is conserved and thus leads to comparable energy densities ε. Only for the highest D^{ELM} for which the SOL collisionality right after the ELM crash is very large (but the ELM energy loss ΔW^{ELM} is unreasonably high) the classical parallel heat transport is moderated and q_{max}^{norm} becomes similar to expected lower experimental value $q_{max}^{norm,exp}$ ~0.2.

Despite these discrepancies of the JINTRAC model being not able to resemble the details of target condition time evolution in the short period right after the ELM-crash it still can be used to make predictions on ITER-like wall scenarios with ELMs included (i.e. to define an ELM induced sputtered particle source) as long as not too short time-scales are discussed.

3. JET ITER-LIKE WALL PREDICTIONS FOR TYPE-I ELMY H-MODE REFERENCE SCENARIO

In the ILW setup with main-chamber PFCs made of Be and the divertor made of W-coated CFC and bulk-W at the strike-point, carbon will be replaced as the main intrinsic radiating impurity by a combination of beryllium and tungsten (however it is important to note that in Asdex-Upgrade discharges after moving to all-metal PFCs at least 1% carbon concentration has been observed [29]). For technical reasons JINTRAC assumes a slightly different setup for the special case where the outer strike-point is located on the horizontal load bearing septum replacement plate. Only the inner vertical target, the horizontal target and the private flux zone components in between are assumed to be made out of tungsten whilst the main-chamber but also the outer vertical divertor components are assumed to be made out of Be. However, the assumption is reasonable, as the outer vertical target plate shows only minor net erosion in configurations with the outer strike-point on the horizontal target as post mortem analysis from JET campaign 2007-2009 showed [30]. Essentially, all relevant transport parameters were kept the same as for the carbon reference case

(inter- and intra-ELM transport, SOL transport model, MHD critical pressure gradient, auxiliary NBI power, gas-fuelling and pumping efficiency). Due to the absence of the main radiator carbon in the ILW configuration (eroded Be does only have a very low radiation efficiency) an additional amount of seeded neon ranging from a small injection rate of 10^{18} atoms/s up to large values of $2 \cdot 10^{19}$ atoms/s was assumed to adjust the radiation and heat loads towards the targets.

Figure 5 compares the time traces of the total radiated power (core and SOL) of the JINTRAC model with the experimental signal of bolometry. Also shown is the all-carbon reference case with ELMs of 275kJ energy loss for which the total radiated power is underestimated for the inter-ELM phase by a factor of 2 and for the intra-ELM peak by a factor of 5.

In case of the ILW configuration with a moderate neon gas seeding of 10^{19} atoms/s JINTRAC delivers roughly the same level of radiation for the inter-ELM phase as for the all-carbon reference case. The peaking of radiation at ELM time is a factor of 2 lower as for the all-carbon case. Although the radiation in the inter-ELM phase is similar the ELM frequency has decreased by ~30% which is due to the fact that in case of neon seeded plasma more energy is radiated away from the confined region as compared to the unseeded case with only carbon radiating. Hence, the pedestal needs more time for building up again. The effect of decrease of f_{ELM} when switching to seeded plasmas is also observed experimentally [31].

The tungsten erosion flux in the inter- and intra-ELM phase precluding self-sputtering was derived from the Eckstein-formula for physical sputtering [17] taking into account the modelled time-dependent target electron temperature, bulk particle and impurity flux profiles towards the targets as well as the impact angle. Fig. 5 shows the total cumulated number of eroded W particles N_W^{eroded} from inner and outer targets as function of time for a single ELM. The JINTRAC simulations indicate that no tungsten is created in the inter-ELM phase. Starting from the case with very low neon seeding (10^{18} neon atoms/s) at the ELM roughly $N_W^{eroded} \sim 5 \cdot 10^{16}$ or more W atoms per ELM are sputtered, mainly by bulk ions. It is important to note that this crude calculation does neglect the effect of W prompt redeposition and self-sputtering. Moreover since the heat flow towards the target is overestimated as described in the previous section the target temperature at ELM-time and thus W-sputtering is probably overestimated too (in JINTRAC $T_{e,target} \sim 1000$eV at peak).

The actual tungsten transport into the confined region to estimate the core W concentration was not analysed with JINTRAC. In a post-processing way the JINTRAC data in terms of 2D plasma distributions and target fluxes were fed into DIVIMP Monte-Carlo code to assess the W transport kinetically and to include the effect of prompt W-redeposition. DIVIMP calculated W leakage fractions $f_{leak} = \Gamma_W^{core} / \Gamma_W^{gross\text{-}erosion}$ into the core of the order of 5% which takes into account prompt W redepostion of the order 90% (details of DIVIMP simulations are given in [32]). From these results a net number of $N_W^{ELM} = N_W^{eroded} f_{leak} \sim 2.5 \cdot 10^{15}$ W atoms per ELM crash would leak into the core. Dux et al [33] recently presented a regression analysis of an Asdex-Upgrade ELMy H-mode shot series and derived a tungsten particle confinement time scaling[1] $\tau_W = 4 \cdot 10^2 \, f_{ELM}^{-1.1} \tau_{SOL}^{1.1} D_{SOL}^{0.1}$ which includes the effect of flushing of W by ELMs

[1] The regression factor $1.4 \cdot 10^{-2}$ in eq. 14 of [Dux2011] is incorrect and has to be $4 \cdot 10^2$ [35].

out of the confined region into the SOL. With f_{ELM}=15Hz and assuming $\tau_{SOL}=L_{||}/c_{s,}w \sim 0.01$s for the tungsten parallel SOL transport in JET this formula provides an estimate for th JET W core confinement time τ_W~0.1s. Hence an average number of $N_W^{average} = N_W^{ELM} f_{ELM} \tau_W \sim 3.75 \cdot 10^{15}$ tungsten particles would be accumulated in the core giving an average W density $n_W = N_W^{average} / V_{core} \sim 3.75 \cdot 10^{13}$ m^{-3}. Assuming flat core profiles with average $T_e = 2$keV, $n_e = 5 \cdot 10^{19} m^{-3}$ and from standard textbook formula for the tungsten radiative function $R_W(T_e = 2\text{keV}) \sim 5 \cdot 10^{-31} Wm^3$ [34] a rough estimate of the average W core radiated power can be derived: $P_{rad} = n_e n_W R_W V_{core} \sim 100$kW. Increasing the neon seeding rate significantly to $2 \cdot 10^{19}$ atoms/s and assuming again f_{leak} of 5% the net value of W atoms per ELM crash increases to $N_W^{ELM} = N_W^{eroded} f_{leak} \sim 5 \cdot 10^{15}$ and thus the estimate for $P_{rad} \sim N_W^{ELM}$ increases to ~200kW, i.e. doubling the previous value with no or very low neon seeding.

CONCLUSION

The JINTRAC integrated code suite has been used to model interpretatively a low triangular JET type-I ELMy H-mode reference shot assuming an all-carbon first wall and target plates. Despite of shortcomings of the adhoc procedure to describe the nature of the ELMs in JINTRAC, the experimentally observed ELM dynamics in terms of ELM frequency, density and temperature drop, inter- and intra-ELM heat flows towards the targets are reproduced. JINTRAC generally overestimates the maximum heat flux q_{max} resulting from too fast parallel SOL transport times in the fluid model. But integrated over time the energy balance is maintained and the experimental value of normalised energy density and heat load asymmetry (2/3-1/3 to inner/outer target) are well recovered. The 2D fluid modelling of the SOL is reproducing the characteristics of the free streaming approximation of the ELM filamentary parallel transport towards the targets in terms of ELM energy density ε. Also the ELM wetted area $A_{wet} \sim 1m^2$ is well reproduced. The latter increases linearly with ELM energy loss in case of moderately diffusive ELMs. A_{wet} saturates in case of strong convective ELMs.

By assuming the same inter- and intra-ELM transport parameter setup as for the all-carbon reference case, JINTRAC shows in its predictive modelling for the ITER-like wall material combination, Be main chamber and W divertor PFCs, that the missing main radiator carbon can be replaced by a seeding impurity. Roughly the same level of radiation can be achieved by applying the neon gas seeding to small quantities ($1 \cdot 10^{19}$Ne/s) levels. From the 2D flow and plasma profiles at the targets the cumulated eroded tungsten material has been estimated. W is sputtered in equivalent parts by bulk deuterium and neon ions for the reference scenario. Per ELM an order of 10^{16} eroded W particles were estimated. Under the assumption that only 5% of gross eroded W is ultimately leaked into the confined region as calculated by DIVIMP the range of core accumulated tungsten radiated power P_{rad} is estimated to be starting from 100kW (erosion by main plasma ions only) up to 200kW depending on the amount of seeded neon impurities. Compared to the auxiliary power necessary to exceed the LH-transition threshold however (in JET Pulse No: 73569 $P_{NBI} = 13$MW

was applied) this level of radiation is not too significant. Thus it is predicted that the operation in terms of a H-mode access with the new JET ITER-like metal wall in place is not critical. The model has shown that the existence of seeded impurities has an effect on the core confinement though, ELM-frequency has decreased by 30% due to larger heat losses of the ETB in the inter-ELM phase. A more rigorous validation and verification of the JINTRAC modelling results including DIVIMP calculations for type-I ELMy H-mode JET scenarios in ILW configuration is planned for the forthcoming JET experimental campaigns.

ACKNOWLEDGEMENTS

This work was supported by EURATOM and carried out within the framework of the European Fusion Development Agreement. The views and opinions expressed herein do not necessarily reflect those of the European Commission.

REFERENCES

[1]. J. Pamela, et al., An ITER-like wall for JET, Journal of Nuclear Materials **365-366** (2007) 1
[2]. S.Brezinsek et al., Journal of Nuclear Materials (2010), article in press doi:10.1016/j.jnucmat.2010.12.097
[3]. S.Wiesen, et al., JINTRAC-JET modelling suite, JET ITC-Report 2008, http://www.eirene.de/JINTRAC_Report_2008.pdf
[4]. A. Taroni et al., in: Proc. 16th IAEA Int. Conf. on Fusion Energy (Montreal, Canada, 7–11 Oct 1996) vol **2**, p 477
[5]. G. Cennachi, A. Taroni, JET Report JET-IR(88)03 (1988)
[6]. Lauro-Taroni L, et al., Proc. 21st EPS conf. on Controlled Fusion and Plasma Physics, Montpellier (1994) 102
[7]. R. Simonini et al., Contribution to Plasma Physics **34**, 368 (1994)
[8]. D. Reiter, Journal of Nuclear Materials, **196-198**:241 (1992), http://www.eirene.de
[9]. S.Wiesen, EDGE2D/EIRENE code interface report, JET ITC-Report 2006, http://www.eirene.de/e2deir_report_30jun06.pdf
[10]. P.M. Stubberfield and M.L. Watkins, JET Internal Report, DPA(06)/87 (1987) .
[11]. Erba M., Cherubini A., Parail V., Sprigmann E. and Taroni A. Plasma Physics and Controlled Fusion **39** (1997) 261
[12]. W. Houlberg et al., Physics of Plasmas **4** (1997) 3231
[13]. J. Lonnroth et al., Contribution to Plasma Physics **46**, (2006) 726
[14]. S.Wiesen et al, Contribution to Plasma Physics **48**, No. 1-3, (2008) 201
[15]. W.Fundamenski, et al., Journal of Nuclear Materials **313** (2003) 787
[16]. A.Kallenbach, et al., Plasma Physics and Controlled Fusion **46** (2004) 431
[17]. W. Eckstein, Garcia-Rosales C., J. Roth, et al. Sputtering data. MPI-Garching, February 1993
[18]. J. Roth. Journal of Nuclear Materials, **266-269** (1999) 51
[19]. S.Tamor, Journal of Computational Physics **40,** (1981) 104

[20]. S.J.P. Pamela, G.T.A. Huysmans, et al., Plasma Physics and Controlled Fusion **53** (2011) 054014
[21]. M.N.A.Beurskens, et al., Nuclear Fusion **49** (2009) 125006
[22]. T. Eich et al., Plasma Physics and Controlled Fusion **49** (2007) 573
[23]. T.Eich, et al., Journal of Nuclear Materials (2010), article in press doi:10.1016/j.jnucmat.2010.11.079
[24]. S.Jachmich, et al., Journal of Nuclear Materials (2010), article in press doi:10.1016/j.jnucmat.2010.12.015
[25]. W.Fundamenski, R.Pitts, et al., Plasma Physics and Controlled Fusion **48** (2006) 109
[26]. D.Tskhakaya, et al., Journal of Nuclear Materials **390–391** (2009) 335
[27]. H.Thomsen, et al., Power load characterization for Type-I ELMy H-Modes in JET, PSI 2010 San Diego, submitted to Nuclear Fusion
[28]. E. Havlickova et al, (2011) submitted to Plasma Physics and Controlled Fusion
[29]. R. Neu, et al., these proceedings
[30]. J. Likonen et al., proc. 13th PFMC 2011, Rosenheim, Germany subm. to Physica Scripta
[31]. C. Giroud, et al., 23rd IAEA Fusion Energy Conference, Daejon, Korea (2010)
[32]. A. Jaervinen, these proceedings
[33]. R. Dux, et al., Nuclear Fusion **51** (2011) 053002
[34]. J. Wesson, et al., Tokamaks, 3rd Ed., Clarendon Press Oxford, (2004) 230
[35]. R. Dux et al., private communication

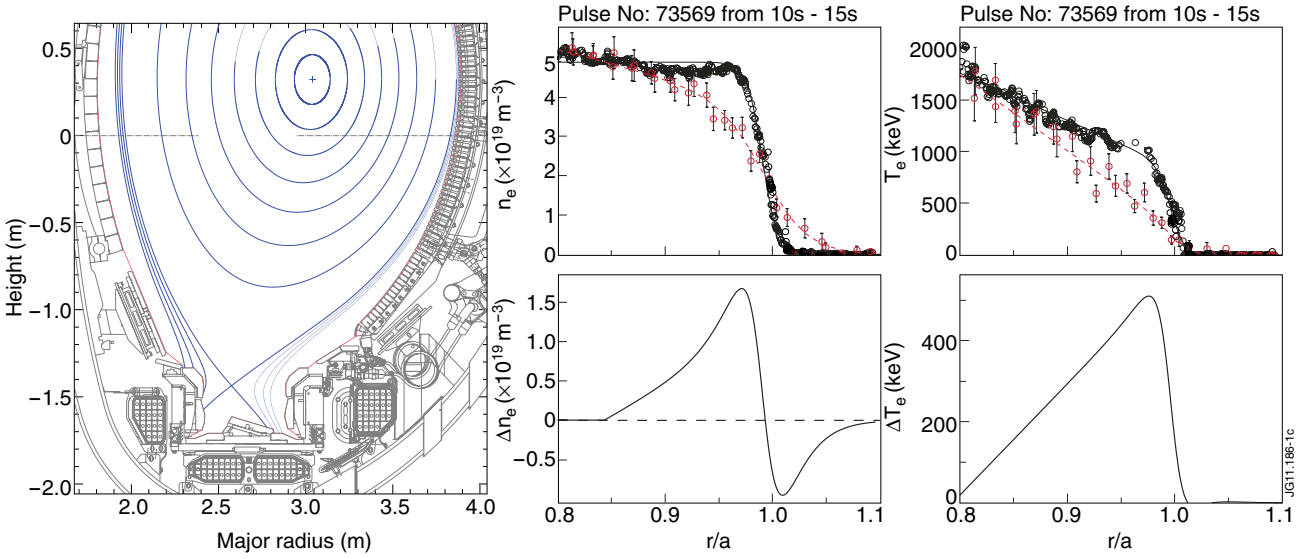

Figure 1: Left : JET Pulse No: 73569, Right : ELM profile dynamics from ELM syncronized HRTS data for JET Pulse No: 73569. Black: pre-ELM profile between 3ms and 0.1ms before ELM. Red : post-ELM selected profiles between 0.2 and 1ms after ELM crash (taken from Beurskens et al [Beurskens2009], copyright Nuc.Fusion).

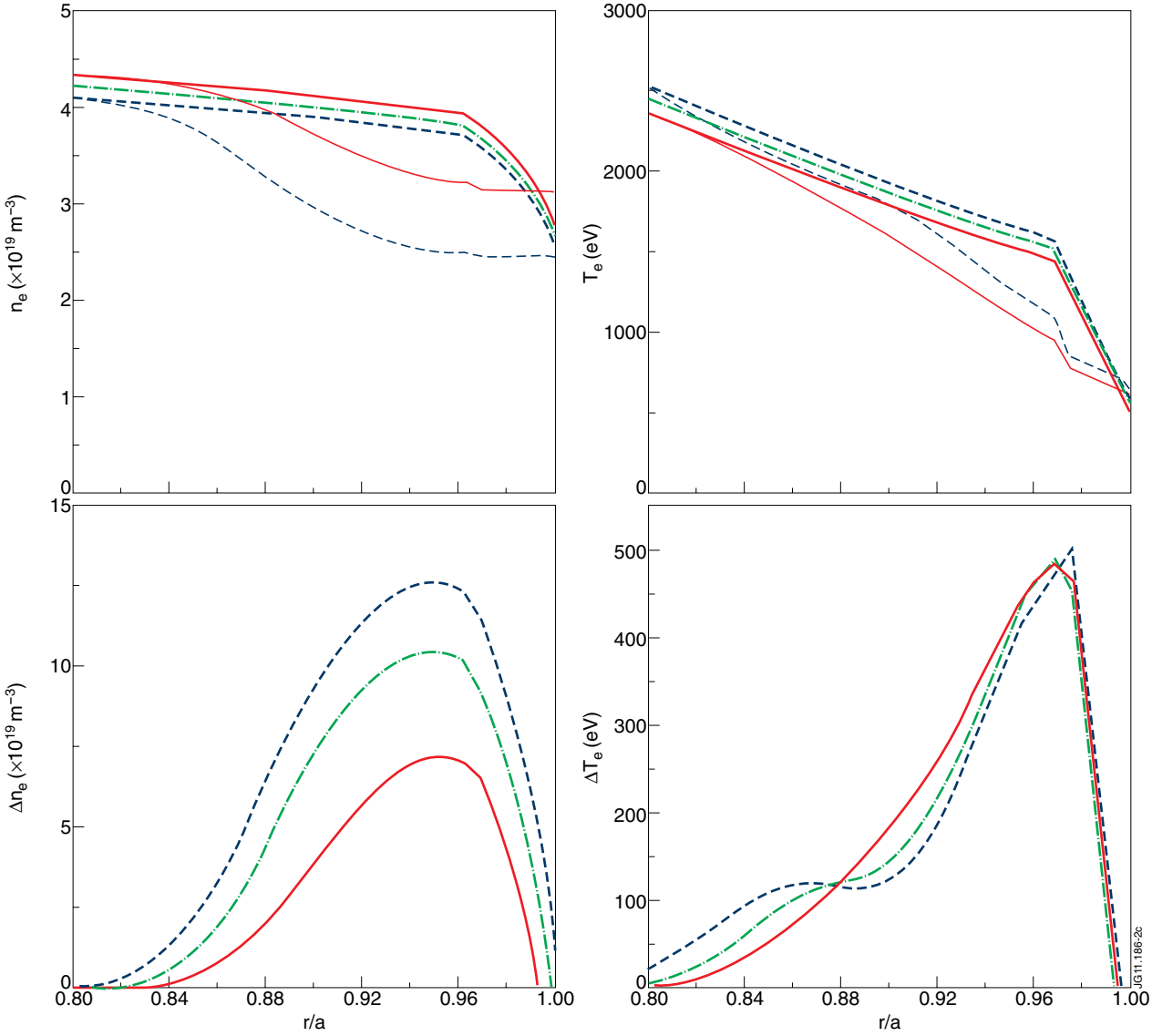

Figure 2: JINTRAC modelling results of pre- and post electron density and temperature profiles at the outer midplane to be directly compared with the experimental profiles in fig.2. Shown are the three cases as decribed in the text with increasing ELM diffusivity D^{ELM}. W^{ELM}=275kJ, 371kJ and 466kJ for red, green and blue respectively.

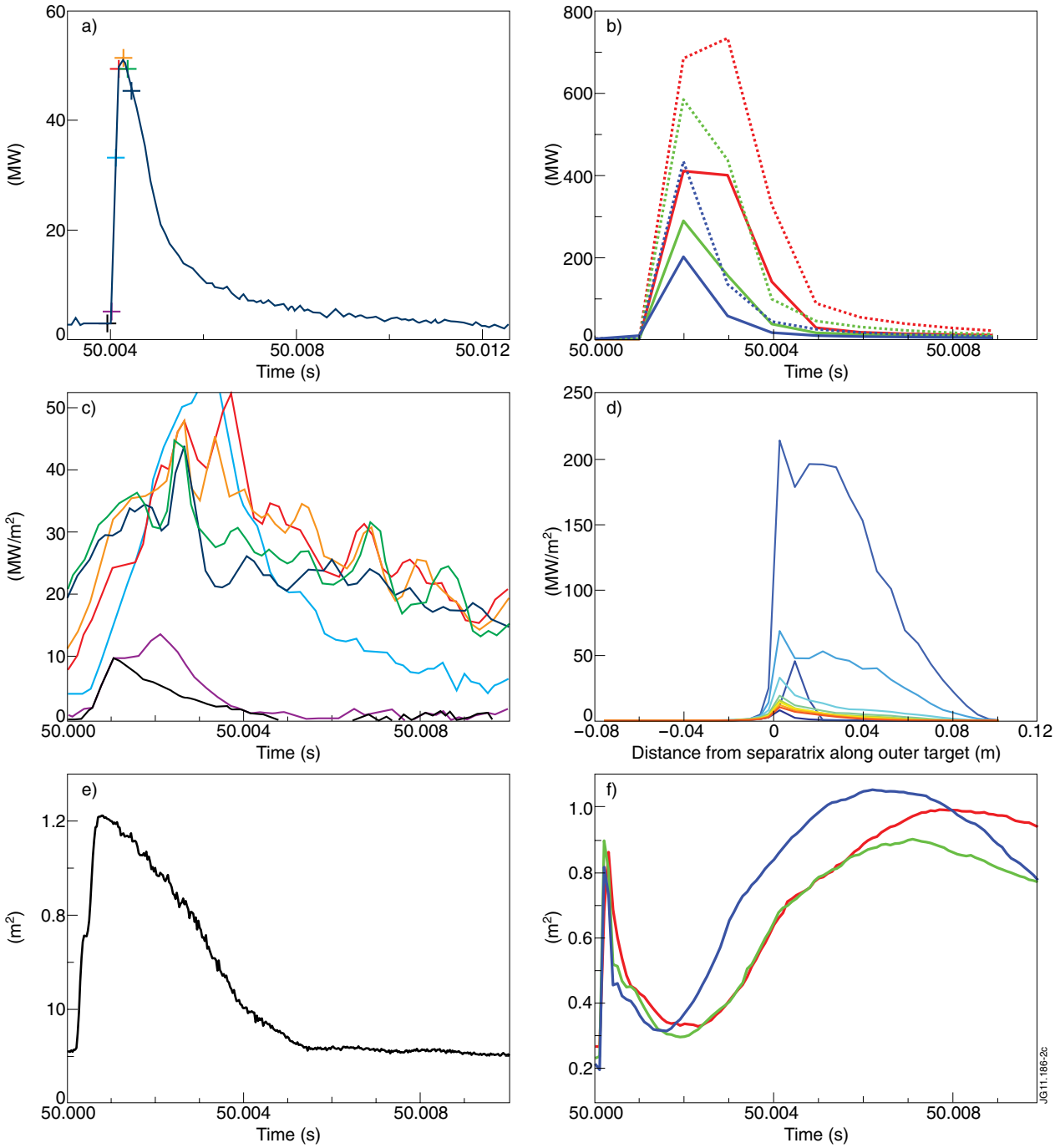

Figure 3: (a): transient of total power arriving at horizontal target plate of JET Pulse No: 73569 measured by IRTV for a single ELM @t=50.004 secs (time axis is shifted by 40secs), (b) JINTRAC results for power arriving at outer (solid) and inner target (dashed). Note the much faster decay time compared to experiment. Plotted in red, green and blue are the three cases with increasing ELM induced diffusion D^{ELM} with W^{ELM}=275kJ, 371kJ and 466kJ respectively. (c) IRTV outer target heat flux profiles for selected times, colors correspond to markings in (a). (d): heat flux profiles modelled by JINTRAC for the case with W^{ELM}=466kJ. Each profile shown is separated by $\Delta t=10^{-4}$s. The low lying dark blue line with peak value 10MW/m^2 correspond to the inter-ELM phase heatflux. (e): IRTV outer target ELM wetted area $A_{wet}(t)=P(t)/q_{max}(t)$ averaged over all ELMs between t=50s and 56s. (f): JINTRAC ELM wetted area $A_{wet}(t)$ for the three cases plotted with 10 times coarser time-resolution compared to (a).

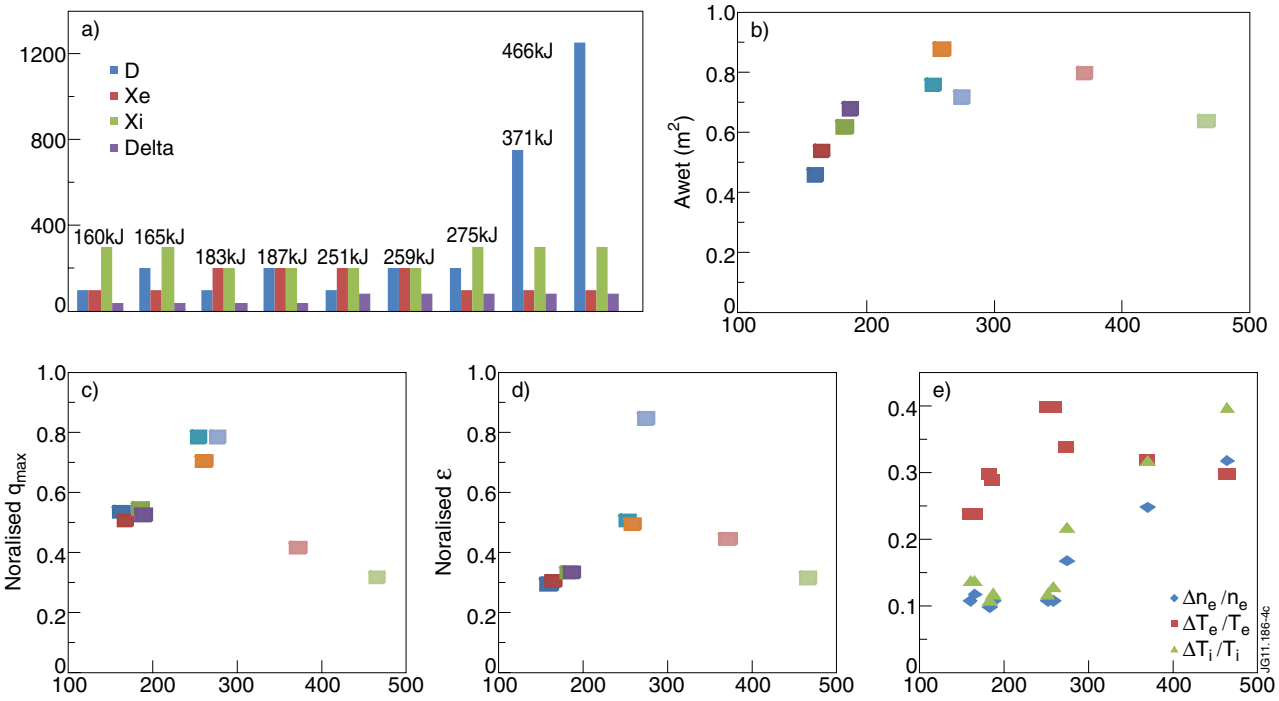

Figure 4: (a): bar chart displaying ELM characteristics in JINTRAC in terms of D^{ELM}, $\chi_{e,i}^{ELM}$, Δ^{ELM} with increasing ELM size W^{ELM} from left to right. (b): peak ELM wetted area A_{wet} for all cases. (c): normalised quantities for maximum heat flux $q_{max}^{norm} = q_{max}/p^{ped}/c_s^{ped}/min(1,\tau_{ELM}/\tau_{||})$ and (d) energy density $\varepsilon^{norm} = \varepsilon/L_{||}/p^{ped}$. To recalculate the unormalised quantities one needs to multiply q_{max}^{norm} and ε^{norm} with $7.62 \cdot 10^9$ [W/m²] and $1.16 \cdot 10^6$ [J/m²] respectively. (e): relative pedestal drops $\Delta n_e/n_e$, $\Delta T_e/T_e$ and $\Delta T_i/T_i$ taken at r/a = 0.95.

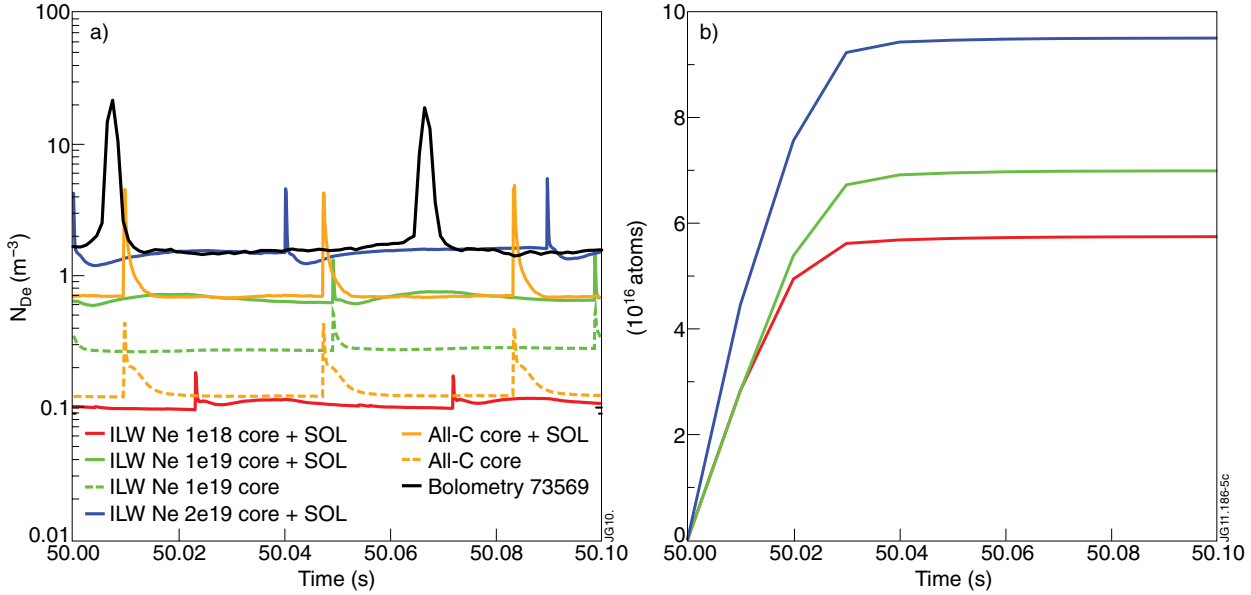

Figure 5: (a): Total radiated power (core and SOL) taken from bolometry for JET shot 73569 compared to JINTRAC all-carbon reference (W^{ELM}=275kJ) case and ILW prediction cases of neon seeding scan. Shown with dashed lines are the fractions of the core radiation only for the all-carbon and moderate neon seeding cases. (b): cumulated tungsten eroded particles from inner and outer target plates of ILW predictive neon-seeding scenarios per ELM (red: 10^{18}, green: 10^{19}, blue: $2 \cdot 10^{19}$ neon particles/s). The red case can be regarded as with W-sputtering due D-impact only.